Vertically Averaged Models for CO_2 Storage in Porous Media

Master of Science Thesis in Applied and Computational Mathematics

Andreas Hammer

Matematisk Institutt
Universitetet i Bergen

November 2008

Preface

I would like to thank my supervisor Jan Martin Nordbotten for being a nice guy, and for helping and guiding me through the years of my master studies. To family and friends, thank you for the encouragements and support.

Contents

Chapter 1

Introduction

It is widely accepted in the academic community that the ongoing climate changes are caused by humans. The main factor of the increase of global warming is the increase of the greenhouse effect due to the emission of CO_2 into the atmosphere. CO_2 is naturally in the atmosphere together with steam and other gases, but the extensive use of fossil fuel such as coal, oil and gas has increased the concentration of CO_2 compared to the other gases. An increase of the concentration of CO_2 in the atmosphere will lead to an increase of the temperature which causes glacier retreats and Arctic shrinkage which in turn will cause the sea level to rise. Other effects of higher concentration of CO_2 include acidification of water, generally worse climate and more extreme weather [2].

From the beginning of the industrial age and up to 1985 the atmospheric concentration of CO_2 increased by 31% [14], subsequently, we have observed an average annual increase of 1.7 ppm (parts per million) in volume [19] measured at the Mauna Loa Observatory in Hawaii (see figure 1.1). The amount of CO_2 in the atmosphere is today approximately 385 ppm. The concentration may reach from 541 to 970 ppm by 2100 if the burning of fossil fuel continues as before, according to a number of different climate models [17].

There are different ways of dealing with the issue. First, it is important to recognise that burning of fossil fuel will continue for many years to come. Countries such as China are developing fast, and the demand of energy will most likely increase for both the industry and in the homes of regular people.

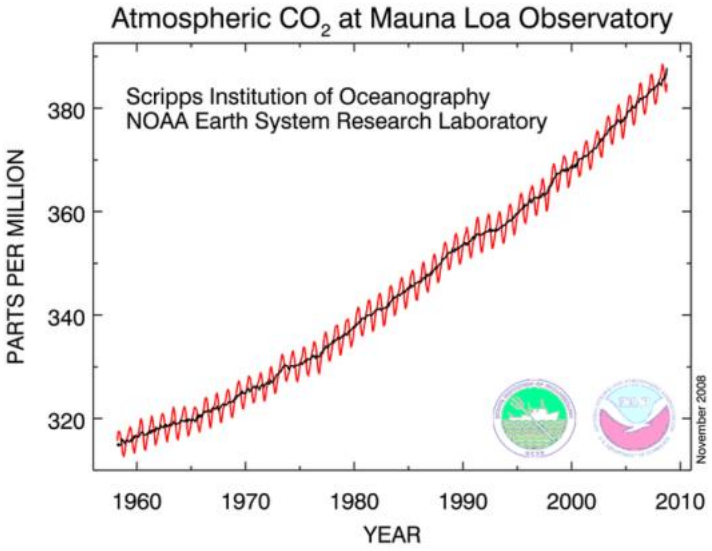

Figure 1.1: [19]

In China alone, one to two coal power plants are starting up each week [4], thus it can be expected that the concentration of CO_2 in the atmosphere will increase unless something is done to prevent it.

The *clean* technologies such as solar, wind, geothermic, nuclear and hydro technology all contribute to produce energy without burning fossil fuel. These projects must be developed further since all this technology combined is today not enough to produce the energy needed. While we develop efficient *clean* technology, a large majority of the energy will be provided by power plants that emit CO_2. In order to mitigate global warming and maybe other consequences still unknown something must be done to stabilise or hopefully reduce the concentration of CO_2 in the atmosphere. Several actions must be taken at the same time since there is not one mean that can solve the problem alone. This thesis concerns one of the many solutions, namely capture and storage of CO_2.

It is hard to capture the CO_2 produced in for instance transportation(cars, airplanes, ships), but the CO_2 emitted by a power plant is easier to capture . In a power plant large amounts of CO_2 are emitted within a small area, and the power plant may therefore be referred to as a *point source*. Other point sources are oil and gas production sites that produce oil and gas containing CO_2. Supposing the CO_2 can be captured at point sources, now the next question is where to store it. Storing CO_2 deep in the oceans or outside

the atmosphere has been suggested, but this is difficult both technologically, economically and politically. The most promising solution to the problem, appears to be to capture and store CO_2 in underground geological formations.

The geological formations that are suited for the CO_2 storage consist of porous rocks such as sandstone. The void space in the porous rock may be filled with fluids. An advantage in considering these formations is that for more than 150 years oil and gas have been produced from such formations, so there is already a significant amount of research done in this field and the technology and equipment needed already exist. An other point is that leakage of CO_2 back into the atmosphere is not really a problem since hydrocarbons and ground water have been stored in such geological formations for millions of years and thereby proved that the formations are sealed. This is only partially true since many of the suited storage formations are perforated by old wells used during the production of hydrocarbons. In order for the CO_2 to stay in the formation, the reservoir must have a seal of a low-permeable rock on top of the reservoir. We will not consider leakage problems, even though that is one of the main concerns of geological storage of CO_2.

CO_2 has already been used for several decades in enhanced oil recovery, but in 1996 Statoil started a pilot project storing CO_2 in Utsira formation containing mineralized water under the seabed in the North Sea (see figure 1.2). Because of the high concentration of minerals and salts, the water is not usable for humans so no drinking water is polluted. This project shows that it is possible to store CO_2 in such formations.

The main advantage of using an aquifer instead of an oil field is the capacity. Around the world there is considered to be enough room for between 1000 Gt and possibly $O(10^4)$ Gt of CO_2 in deep saline formations while the oil and gas fields have a maximum capacity of 900 Gt [17].

At sufficiently high pressures, the density of CO_2 is increased drastically compared to its density at atmospheric temperature and pressure. Therefore if CO_2 is injected into a deep enough formation, the volume needed to store the gas is reduced. The typical depth of such a formation is 800 m below sea level or lower, and the temperature and pressure at such depths causes the CO_2 to have a supercritical nature.At ideal conditions there will be little leakage of CO_2 from the reservoir and a report from the Intergovernmental Panel on Climate Change states that it is likely that 99% of the injected CO_2 still is in the reservoir after 1000 years [17].

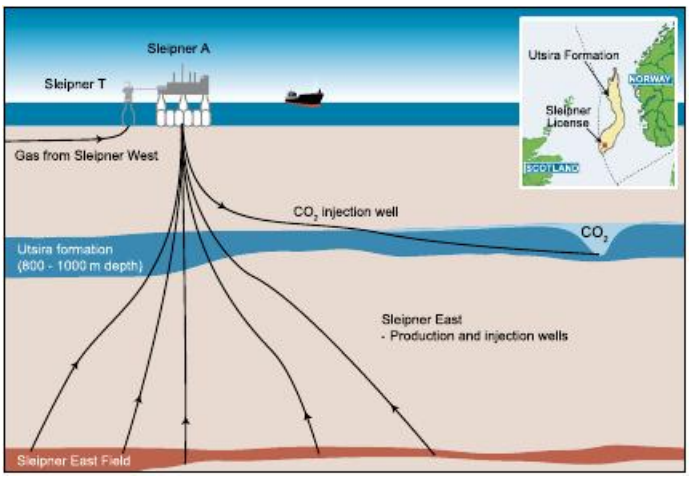

Figure 1.2: CO_2 storage in the North Sea [17]

In order to understand the behaviour of the CO_2 in the geological formation, it is important to do calculations and run simulations. The oil and gas industry has developed powerful software to simulate the flow in oil and gas fields. These programs can simulate multi phase physics in 3 dimensions and they give a good picture of the physics in the reservoir. However when CO_2 is injected into an aquifer, large areas need to be considered. The typical aquifer has a height of tenths of meters and a width on the kilometer scale. To run a full 3D simulation of an area that big takes a lot of computational resources and time. We are interested in studying simplifications that might make it possible to do the same simulation in only 2 dimensions and thereby save a lot of computation power and time and still get a good 3D result.

A traditional approach is to use a vertically integrated model. This was a commonly used simplification in the oil and gas industry before more powerful computers were developed. The goal of the model is to take the averages of the variables in the vertical dimension and use the averages in the model as if the reservoir is completely horizontal. The big density difference between the saline water and the CO_2 helps construct the method and in most cases the fluids are assumed to be in vertical hydrostatic equilibrium [9, 8, 7, 10]. The vertical equilibrium assumption says that the fluids are assumed to flow only horizontally and not vertically. This is a rather strong assumption limiting the physics in the reservoir. It may be a good assumption in many cases but it has also been shown that there are cases where it is not [15]. Particularly in areas around wells the vertical flow is of importance.

In this thesis we wish to implement and simulate both the case of no vertical flow of the fluids, *vertical equilibrium assumption*, and the case where the fluids may flow vertically. We will refer to the latter as the *structured vertical velocity approximation*. The advantage of assuming that the fluids are in vertical equilibrium is that we can save a lot of computational time, but intuitively the non-equilibrium model gives a more correct picture of the flow in the reservoir.

In chapter 2 we set up the mathematical model we use to simulate the flow in the aquifer. We continue in chapter 3 by introducing the vertically averaged models. Chapter 4 contains some calculations and discretization methods of the equations obtained in chapter 4. Problems and challenges involving the implementation in Matlab are also discussed in chapter 4. Numerical examples of the implemented code is presented in chapter 5 and the discussion and results are in chapter 6.

Chapter 2

Mathematical Model

The brine[1] in the aquifer is located in the pores of a porous rock formation. To set up a model we look at physical laws of the rock and the fluids flowing inside the rock. The mathematical model used in this thesis is based on two-phase flow described in Pettersen's book [18]. We start out with some well known equations and assumptions and end up with a model describing the behaviour of the two phases, CO_2 and brine.

2.1 Darcy's Law

Darcy's law deals with flow velocity of fluids in porous media. First let us look at some properties of the porous rock.

2.1.1 Porosity

The volume of the void space divided by the total volume of the rock is referred to as the rocks porosity,

$$\phi = \frac{V_{pores}}{V_{total}}$$

The porosity represents the volume fraction that can be occupied by a fluid in the rock.

[1]Brine is water with high concentration of salt, and contains more than 50 ppt (parts per thousand) of salt in volume.

2.1.2 Permeability

Another property of the porous rock is the permeability. Permeability $\mathbf{K}$ describes the conductivity of a rock in different directions, and mathematically it is a second order tensor. A different way to view permeability is to consider $\mathbf{K}^{-1}$ as an expression for the resistance the fluid encounters when flowing through the medium. We can compare this with the resistance an electric current meets in an electric circuit.

The nature of a porous rock is complex. The pores are winding through the rock and the size of the pores are very variable, so calculating the exact velocity of a fluid is rather difficult. Darcy's law is an empirical law discovered through laboratory experiments done by the french engineer Herny Darcy (1803-1858). The conclusion of the experiments was that the flow velocity of the fluids in a porous medium is proportional to the pressure difference in the medium.

$$\mathbf{v} = -\frac{\mathbf{K}}{\mu}(\nabla p - \nabla \rho g z) \tag{2.1}$$

Here p is the pressure in the fluid and μ denotes the fluid's viscosity. ρ represents the density of the fluid and g is the gravitational constant acting in the vertical direction z.

A quick analysis of the expression gives us a physical understanding of the flow velocity $\mathbf{v}$. It is the pressure differences in the reservoir that cause the fluids to flow. The effect of gravity only influences the vertical flow since the gravitational constant is multiplied by vertical unit vector. Fluids flow faster in high permeable media, fluids with low viscosity flow faster than fluids with higher viscosity and the higher the pressure difference is, the faster the fluids flow.

2.2 Two-phase Flow

For the rest of this thesis we will use the term phase[2] associated with CO_2 and brine.

[2] A phase may contain several components. Under high pressure can for instance gas be a component in the oil phase but at lower pressure the gas evaporates from the oil and forms a new phase.

2.2.1 Saturation

The saturation S_α, of a phase describes the volume fraction occupied by the phase α and the total volume in a given area. The void space is occupied by either CO_2, brine or both and the sum of the saturations of the phases is equal to one.

$$S_c + S_b = 1$$

where $c = CO_2$ and $b =$ brine.

2.2.2 Relative Permeability

When there is more than one phase present in the reservoir the flow properties seen in (2.1) change. If some of the pore volume is occupied by one phase then there is less space for the other phase to flow in. To correct for the reduction of pore space the relative permeability is introduced. The permeability mentioned above describes only the rock's property and how it effects the flow, while the relative permeability describes how the flow is effected when two or more phases interact with each other. The relative permeability is dependent on the saturation of the phases, and there are many ways to define it. In many oil production models the Corey-type approximation is used for the problem where water is injected into an oil reservoir as pressure support to enhance the recovery of oil, [1]

$$\begin{aligned} k_{r\alpha} &= k_{r\alpha}(S^*) \\ S^* &= \frac{S - S_{wc}}{1 - S_{or} - S_{wc}} \end{aligned} \tag{2.2}$$

Here S_{wc} and S_{or} refers respectively to the connate water and the immobile oil saturation. The same approximation can be used for the case of CO_2 injection into an aquifer containing brine.

The effective permeability in the reservoir is the product of the permeability related to the rock and the relative permeability related to the phases. For simplicity we introduce the mobility λ of the phases,

$$\lambda_\alpha = \frac{k_{r\alpha}}{\mu_\alpha}$$

The Darcy velocities for the different phases when they are both present in the reservoir then become

$$\mathbf{v}_\alpha = -\mathbf{K}\lambda_\alpha(\nabla p_\alpha - \rho_\alpha g \nabla z) \tag{2.3}$$

2.2.3 Capillary Pressure

Now we have two equations that, given initial and boundary conditions, can model two-phase flow in a 3 dimensional porous medium. Capillary pressure is used to close the model. At the interface between two different phases there are forces working due to the different properties of the phases. There will be a pressure jump across the interface caused by the surface tension at the interface.

$$p_{\text{cap}} = p_{\text{non-wetting}} - p_{\text{wetting}}$$

Capillary pressure is dependent on the saturation of the phases since there is no capillary pressure when only one of the phases is present.

$$p_{\text{cap}} = p_{\text{cap}}(S)$$

In the pressure equation we need to calculate gradient of the capillary pressure. The capillary pressure is dependent only on saturation, so the usual way to calculate the capillary pressure gradient is to use the chains rule.

$$\nabla p_{\text{cap}}(S) = \frac{dp_{\text{cap}}}{dS} \nabla S$$

2.2.4 Continuity Equation

For both phases a continuity equation can be introduced. The continuity equation gives for each phase [18]

$$\frac{\partial}{\partial t}(\phi \rho_\alpha S_\alpha) + \nabla \cdot (\rho_\alpha \mathbf{v}_\alpha) = q_\alpha \tag{2.4}$$

where q is a source or sink term. The physical meaning of the expression is that for any volume in the reservoir the change of the saturation of a phase is balanced by the volume-flux of the phase over the boundary the source inside the volume. When there is no source or sink inside the volume then $q = 0$, and the expression states that the change in saturation is equal to the difference of the inflow and outflow of the phase(see figure 2.1).

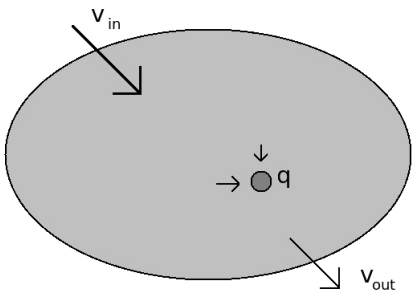

Figure 2.1: Change of saturation balanced by flow across the boundary and the source in an arbitrary volume

2.2.5 Assumptions

In order to set up a closed model for two-phase flow some assumptions need to be made. We want to reduce the number of variables to be able to solve the equations, but at the same time have a model that is able to capture the important physics in the reservoir. In this model we assume that we are dealing with:

- Two immiscible fluids with constant viscosity
- The phases are incompressible

2.2.6 Pressure Equation

If we sum the continuity equations for both the CO_2 and the brine phase, and use the fact that $S_c + S_b = 1$ and the incompressibility assumption we get that

$$\nabla \cdot (\mathbf{v}_c + \mathbf{v}_b) = q \qquad q = q_b/\rho_b + q_c/\rho_c.$$

By inserting the expressions from Darcy's law (2.3) into the equation above we get

$$-\nabla \cdot (\mathbf{K}\lambda_c(\nabla p_c - \rho_c g \nabla z) + \mathbf{K}\lambda_b(\nabla p_b - \rho_b g \nabla z)) = q$$

The next step is to introduce the capillary pressure to reduce the number of unknowns in the equation. The brine pressure is substituted by the capillary pressure, $p_{cap} = p_c - p_b$. The capillary pressure is a function of saturation and can be calculated. The result is the *Pressure equation* with only one unknown variable, p_c.

$$-\nabla \cdot \mathbf{K}\lambda_T \nabla p_c = q - \nabla \cdot \mathbf{K}\lambda_b \nabla p_{cap} - \mathbf{K}\lambda_T(\rho_b + \rho_c)g\nabla z \tag{2.5}$$

where the total mobility $\lambda_T = \lambda_c + \lambda_b$.

2.2.7 Saturation Equation

Now we have an equation that only contains the CO_2 pressure. Next we want an equation that only depends on other CO_2 parameters. By inserting the CO_2 pressure obtained in the pressure equation into Darcy's law we get the CO_2 flow velocities. Further we use those velocities in the continuity equation for the CO_2 phase:

$$\phi \frac{\partial S_c}{\partial t} + \nabla \cdot \mathbf{v}_c = \frac{q_c}{\rho_c} \tag{2.6}$$

This is the so-called *Saturation equation* for the CO_2-phase.

By combining the pressure equation (2.5), Darcy's law (2.3) and the saturation equation (2.6) we can calculate and simulate the flow and saturation changes in the reservoir.

Chapter 3

Vertically Averaged Formulation

The mathematical model described in the previous chapter is the general model used to simulate 3-dimensional flow of phases in a porous media. We wish to reduce the amount of calculations needed and we do so by introducing an integrated model. Since the vertical length scale is much smaller than the horizontal length scale, we choose to integrate the model vertically to obtain the 2-dimensional model. We want to average all the information and parameters in the vertical direction and present an approximation for the full reservoir in 2 dimensions.

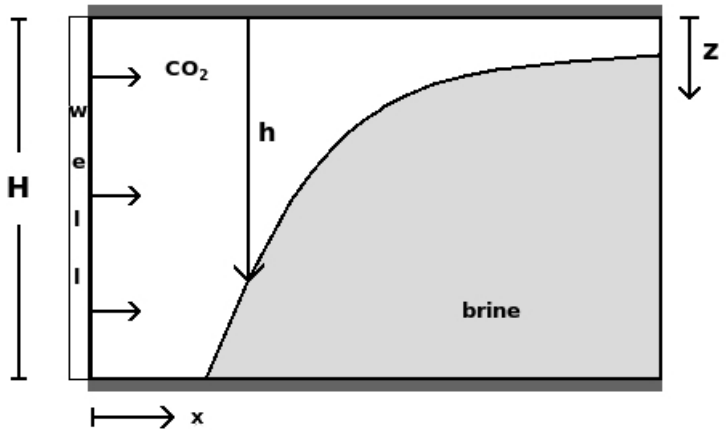

Figure 3.1: A vertical cut of a reservoir where CO_2 is injected

Because of the big difference in the density and the following gravity override (see figure 3.1, we can assume that the phases we study are separated by a sharp macroscopic interface at height $z(t) = h(x, y, t)$. In reality however, CO_2 and brine are slightly miscible but the effect of that is not what we want to study in this thesis, so we ignore the drying front between the two phases.

We also assume that the reservoir is horizontal an has constant height H.

During the injection the CO_2 displaces the brine and flows to the top of the formation. For simplicity we assume that the residual saturation of brine is zero, meaning that the CO_2 fully displaces the brine. The saturations of the phases as function of the height are then given as:

$$S_c = \begin{cases} 1 & 0 < z < h \\ 0 & h < z < H \end{cases} \tag{3.1}$$

$$S_b = \begin{cases} 0 & 0 < z < h \\ 1 & h < z < H \end{cases} \tag{3.2}$$

We continue with the continuity equation for each of the phases, and integrate them over the vertical thickness of the phase. The top of the reservoir is located at $z = 0$ and the positive vertical direction is chosen to point downward so the bottom of the reservoir is at $z = H$. For the CO_2 phase we get:

$$\int_0^h \phi \frac{\partial S_c}{\partial t} \mathrm{d}z + \int_0^h \nabla \cdot \mathbf{F}_c \mathrm{d}z = \int_0^h \frac{q_c}{\rho_c} \mathrm{d}z \tag{3.3}$$

The integrated continuity equation for the brine phase is:

$$\int_h^H \phi \frac{\partial S_b}{\partial t} \mathrm{d}z + \int_h^H \nabla \cdot \mathbf{F}_b \mathrm{d}z = \int_h^h \frac{q_b}{\rho_b} \mathrm{d}z \tag{3.4}$$

In the integrated equations above $\mathbf{F}_\alpha$ are functions of the pressure and the saturation in 3 dimensions and describes the flux of S_α.

$$\mathbf{F}_\alpha = \mathbf{F}_\alpha\big(S_\alpha(x, y, z, t), P_\alpha(x, y, z, t)\big) \tag{3.5}$$

To further simplify the model we assume that the porosity is constant in the vertical direction.

We continue with the equations for the CO_2. By the assumptions above the first term of equation (3.3) becomes:

$$\int_0^h \phi \frac{\partial S_c}{\partial t} \mathrm{d}z = \phi \frac{\partial}{\partial t} \int_0^h 1 \mathrm{d}z = \phi \frac{\partial h}{\partial t} \tag{3.6}$$

The vertically averaged continuity equation for the CO_2 phase is then new continuity equation for the variable h:

$$\phi \frac{\partial h}{\partial t} + \nabla \cdot \int_0^h \mathbf{F}_c \mathrm{d}z = \int_0^h \frac{q_c}{\rho_c} \mathrm{d}z \tag{3.7}$$

To reduce the system of equations to a system of only 2 dimensions we seek to express $\mathbf{F}_c$ as a function of the variable h and the pressure at a fixed height in the reservoir, for instance at the top:

$$\int_0^H \mathbf{F} \approx \hat{\mathbf{v}}(h, p_{\text{top}}) \tag{3.8}$$

The solution strategy is to find an expression for the pressure variation in the vertical direction. Once that is found we can insert the expression into Darcy's law and integrate over the thickness of the phase. Then we should end up with an expression for the vertically integrated horizontal fluxes given as functions of the pressure at a fixed z and the pressure variation based on the location of h. For the CO_2 phase:

$$\hat{\mathbf{v}}_c(h, p_{\text{top}}) = -\int_0^h \frac{Kk_{rc}}{\mu_c} \nabla_{x,y} p_c(z) \mathrm{d}z \tag{3.9}$$

3.1 Pressure derived from Darcy's law

To find an expression for the variation of the pressure in the vertical direction, Darcy's law (2.3) is rearranged:

$$\frac{\partial p_\alpha}{\partial z} = -\frac{\mu_\alpha v_{z,\alpha}}{K_z k_{rz}} + \rho_\alpha g \tag{3.10}$$

Now we integrate the pressure derivative. To find the pressure in the CO_2 phase we simply integrate over the thickness of the CO_2 phase.

$$\int_0^z \frac{\partial p}{\partial z}\, \mathrm{d}z = \int_0^z \frac{\partial p_c}{\partial z}\, \mathrm{d}z, \quad z < h \tag{3.11}$$

Since we have chose the top pressure as the reference pressure in the vertical direction, we integrated from the top to the desired value of z. For the brine phase we must therefore first integrate over the CO_2 phase and then the brine phase.

$$\int_0^z \frac{\partial p}{\partial z}\, \mathrm{d}z = \int_0^h \frac{\partial p_c}{\partial z}\, \mathrm{d}z + \int_h^z \frac{\partial p_b}{\partial z}\, \mathrm{d}z, \quad z > h \tag{3.12}$$

To calculate the integrals above we need an expression for the vertical velocities in the two phases. Of course we could do a full 3 dimensional simulation and simply calculate the velocities based on the pressure, but then the point of integrating the vertical dimension is gone. In order to save computation time and power we must approximate the vertical fluxes.

The question that defines this thesis is: How do we approximate v_z in equation (3.10)?

3.1.1 Vertical Equilibrium Assumption (VE)

In most cases where a similar model is presented, the vertical flow is assumed to be equal to zero [9, 8, 7, 10]. Setting $v_{z,\alpha} = 0$ in (3.10) and carrying out the integration (3.11) and (3.12) yields the vertical equilibrium pressure expression:

$$p(x, y, z, t) = p_{\text{top}} + \begin{cases} +g\rho_c z & z < h \\ +g\rho_c h + g\rho_b(z - h) & z > h \end{cases} \tag{3.13}$$

If we set $z = H$ in the equation above we can find the pressure difference between the top and the bottom of the reservoir, which we choose to define as:

$$\Delta p_{\text{VE}} = g\rho_c h + g\rho_b(H - h) \tag{3.14}$$

This is the same expression as is used when measuring atmospheric pressure below sea level in hydrodynamics. Imagine that p_{top} is the atmospheric pressure at a given height, for instance $H/2$, above sea level and p_{bottom} is the atmospheric pressure at a given depth, $H/2$ in the sea. The distance between the top and bottom is obviously H and the sea surface is the interface between the air and the water. The pressure difference between the point above and the point below sea level is equal to the hydrostatic pressure difference found by using Pascal's law [11]. If the distance between the two points is fixed and both points are moved either up or down the pressure difference between the points change. Since the sea water has higher density than the air, the greatest pressure difference is obtained by setting both points below the surface. This is equivalent to calculating the pressure difference in the reservoir before CO_2 is injected. Similarly the the difference is smallest when both points are above the surface, which is equivalent to the pressure difference in the reservoir when it is fully saturated by CO_2.

Now we have an expression for the pressure variation in the vertical direction, thus we can find the vertically averaged velocities (3.9) corresponding to the continuity equation (3.7). However assuming that the vertical flux is equal to zero is a rather strong assumption that limits the physics in the reservoir. To hopefully get a better picture of the flow, we are interested in the case where the vertical velocities are not assumed to be equal to zero.

3.1.2 Structured Vertical Velocity Approximation (SVV)

We need to approximate the vertical velocities in the reservoir. At the interface between the phases we can set up a boundary condition for the flow of

the two phases. The sketch in figure 3.2 shows the idea behind the boundary condition in 1 dimension.

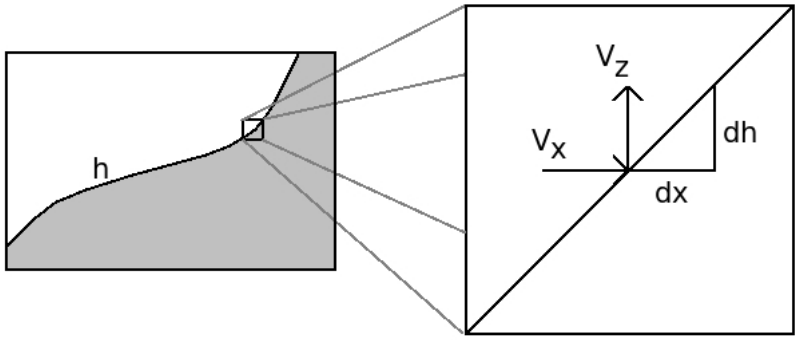

Figure 3.2: Vertical flow related to horizontal flow at the interface of two immiscible fluids

The horizontal flow at the interface is "reflected" vertically at the same rate as the derivative of the interface. We are dealing with two similar triangles so the ratio of the two catheti is equal for the triangles.

$$\frac{v_z|_h}{v_x|_h} = \frac{dh}{dx} \quad \Rightarrow v_z|_h = v_x|_h \frac{dh}{dx} \tag{3.15}$$

If the interface is moving we need to correct for that by adding the term $\phi \frac{\partial h}{\partial t}$.

$$v_{z,\alpha}(h,t) = v_\alpha|_h \cdot \nabla h + \phi \frac{\partial h}{\partial t} \tag{3.16}$$

where $|_h$ means 'at the interface'. The vertical flow at the interface is now given as a function of the horizontal flow at the interface.

However the vertical flow rate is only given on the interface but we can interpolate between the interface and the horizontal boundaries to get an expression for the vertical flow for all z. The reservoir is bounded on the top and bottom so there is no flow over the outer boundaries. We do a linear interpolation that gives us the following result:

$$v_{z,c} = v_{z,c}|_h \left(\frac{z}{h}\right) \qquad z < h \tag{3.17}$$

$$v_{z,b} = v_{z,b}|_h \left(\frac{H-z}{H-h}\right) \qquad z > h \tag{3.18}$$

The vertical velocities are greatest in value on the interface and decrease as we move away from the interface. We can now insert the expressions above into the the rearranged Darcy's law (3.10) and obtain an expression for the vertical pressure variation. Above we made the assumption that the viscosities and densities are constants. Further we assume that the vertical permeability is constant in the vertical direction. The vertical relative permeability is a function of the residual saturation, but since there is no residual saturation the vertical relative permeability is equal to unity. Again we assume that we know the value of the pressure at the top of the reservoir.

$$p(x,y,z,t) = \quad p_{\text{top}} + g\rho_c z - \frac{\mu_c}{2K_z}\frac{z^2}{h}\left(\mathbf{v}_c|_h \cdot \nabla h + \phi\frac{\partial h}{\partial t}\right) \quad z < h \tag{3.19}$$

$$\begin{aligned} p(x,y,z,t) = \quad & p_{\text{top}} + g\rho_c h + \rho_b g(z-h) - \frac{\mu_c}{2K_z}h\left(\mathbf{v}_c|_h \cdot \nabla h + \phi\frac{\partial h}{\partial t}\right) \\ & -\frac{\mu_b}{2K_z}\frac{2H(z-h) - z^2 + h^2}{(H-h)}\left(\mathbf{v}_b|_h \cdot \nabla h + \phi\frac{\partial h}{\partial t}\right) \quad z > h \end{aligned} \tag{3.20}$$

Evaluating the pressure in $z = H$ gives the pressure difference between top and bottom:

$$\begin{aligned} \Delta p_{\text{SVV}} = \quad & g\rho_c h - \frac{h\mu_c}{2\mathbf{K}_z}\left(\mathbf{v}_c|_h \cdot \nabla h + \phi\frac{\partial h}{\partial t}\right) \\ & + g\rho_b(H-h) - \frac{(H-h)\mu_b}{2\mathbf{K}_z}\left(\mathbf{v}_b|_h \cdot \nabla h + \phi\frac{\partial h}{\partial t}\right) \end{aligned} \tag{3.21}$$

In all the equations above (3.19)-(3.21) the height of the interface is dependent on the horizontal location in the reservoir, $h = h(x,y,t)$.

It is not given that the structured vertical velocity approximation non-equilibrium vertical difference is different from the vertical equilibrium vertical pressure difference. There are other ways of defining vertical equilibrium. If the lighter phase flows upward while the denser phase flows downward and the magnitude of the velocities is equal [12], the last part of (3.21) is zero. Vertical equilibrium is also obtained by letting $K_z \to \infty$.

3.2 Integrated Horizontal Flux

The integrated velocity corresponding to the CO_2 phase can now be calculated by equation (3.9):

$$\hat{\mathbf{v}}_c = -\int_0^h \frac{\mathbf{K} k_{rc}}{\mu_c} \nabla_{x,y} p_c \mathrm{d}z \tag{3.22}$$

By the similar argument for the continuity equation for the brine phase, we can calculate the vertically averaged brine velocity.

$$\hat{\mathbf{v}}_b = -\int_h^H \frac{\mathbf{K} k r_{rb}}{\mu_b} \nabla_{x,y} p_b \mathrm{d}z \tag{3.23}$$

We assume that the horizontal permeability is independent of the vertical direction. The horizontal relative permeability is as for the vertical relative permeability equal to one due to the assumed absence of residual saturation. We calculate the horizontal pressure gradient of the pressure now expressed as a function of the height of the interface and the top pressure. Then we integrate the pressure gradient in the vertical direction and we end up with the vertically averaged horizontal fluxes

$$\hat{\mathbf{v}}_c = -\frac{\mathbf{K}}{\mu_c} \int_0^h \nabla p_c \mathrm{d}z. \tag{3.24}$$

$$\hat{\mathbf{v}}_b = -\frac{\mathbf{K}}{\mu_b} \int_h^H \nabla p_b \mathrm{d}z. \tag{3.25}$$

where the vertically averaged horizontal pressure gradients for the structured vertical velocity approximation are:

$$\int_0^h \nabla p_c \mathrm{d}z = h\left(\nabla p_{\mathrm{top}} - \frac{\mu_c h^2}{6K_z} \nabla\left(\frac{\mathbf{v}_c|_h \cdot \nabla h + \phi \dfrac{\partial h}{\partial t}}{h}\right)\right) \tag{3.26}$$

$$\begin{aligned}\int_h^H \nabla p_b \mathrm{d}z = \quad & (H-h)\Bigg[\nabla p_{\mathrm{top}} + \nabla g(\rho_c - \rho_b)h \\ & -\frac{\mu_c}{2K_z}\nabla\Bigg(h(\mathbf{v}_c|_h \cdot \nabla h + \phi\frac{\partial h}{\partial t})\Bigg) \\ & -\frac{\mu_b}{2K_z}\nabla\Bigg(\frac{h^2-2Hh}{H-h}(\mathbf{v}_b|_h \cdot \nabla h + \phi\frac{\partial h}{\partial t})\Bigg) \\ & -\frac{\mu_b}{6K_z}\frac{2H^3-h^2(3H-h)}{H-h}\nabla\Bigg(\frac{(\mathbf{v}_b|_h \cdot \nabla h + \phi\frac{\partial h}{\partial t})}{H-h}\Bigg)\Bigg]\end{aligned} \tag{3.27}$$

For the case of vertical equilibrium we end up with two somewhat simpler expressions:

$$\int_0^h \nabla p_c \mathrm{d}z = h\nabla p_{\mathrm{top}} \tag{3.28}$$

$$\int_h^H \nabla p_b \mathrm{d}z = (H-h)\big(\nabla p_{\mathrm{top}} + g(\rho_c - \rho_b)\nabla h\big) \tag{3.29}$$

We must now choose a reference height for the pressure to calculate the horizontal velocities. We choose to relate the CO_2 flow rate to the pressure at the top, and the brine flow rate to the pressure at the bottom of the reservoir.

$$p_c = p(z=0) = p_{\mathrm{top}} \tag{3.30}$$

$$p_b = p(z=H) = p_{\mathrm{bottom}} \tag{3.31}$$

For simplicity we make the assumption that we can write the vertically integrated phase velocities as functions of the vertical pressure difference between the top and the bottom so that:

$$\int_0^h \nabla p_c \mathrm{d}z \approx h\nabla p_{\mathrm{top}} \equiv h\nabla p_c \tag{3.32}$$

$$\int_h^H \nabla p_b \mathrm{d}z \approx (H-h)\nabla p_{\mathrm{bot}} \equiv (H-h)\nabla p_b \tag{3.33}$$

where we define p_b as

$$p_b = p_c + \Delta p \tag{3.34}$$

and Δp is given by equation (3.13) or (3.21). The velocities then become:

$$\hat{\mathbf{v}}_c = -\frac{Kh}{\mu_c}\nabla p_{\text{top}} \tag{3.35}$$

$$\hat{\mathbf{v}}_c = -\frac{K(H-h)}{\mu_b}\nabla\big(p_{\text{top}} + \Delta p\big) \tag{3.36}$$

The prefixes h and $H - h$, in (3.35) and (3.36) can be viewed as pseudo-relative permeabilities. The local relative permeabilities are equal to unity from the definition on the Corey-type relative permeability(2.2). The prefixes are included in the horizontal relative permeabilities so that:

$$\hat{k}_{r,c} = h \tag{3.37}$$

$$\hat{k}_{r,b} = H - h \tag{3.38}$$

which give the mobilities:

$$\hat{\lambda}_c = \frac{h}{\mu_c}, \quad \hat{\lambda}_b = \frac{H-h}{\mu_b} \tag{3.39}$$

3.3 Vertical Pressure Difference expressed as the Capillary Pressure

From equation (3.11) we get an expression for the vertical pressure difference:

$$\Delta p_z = p_{\text{bottom}} - p_{\text{top}}$$

Since we choose to relate the top pressure to CO_2 and the bottom pressure to brine we can set up a relation between the two phases.

$$\Delta p_z \equiv p_b - p_c$$

This expression looks very similar to the capillary pressure expression we discussed above:

$$p_{cap} = p_{\text{non-wetting}} - p_{\text{wetting}}$$

In the case of CO_2 and brine, CO_2 is the non-wetting phase and brine is wetting. We have already related the pressure in the different phases to each other, but we have not insert that relation into the mathematical model. To do that we substitute the expression for capillary pressure by the the vertical pressure difference.

$$p_{cap} = p_c - p_b = \bar{p}$$

To avoid confusion we will refer to the new "capillary pressure"-expression as the "vertical pressure difference", $\bar{p}$. The meaning of the term ∇p_{cap} has changed from being a local force at the interface to being the sum of the pressure difference between the top and the bottom of the reservoir. Now the vertical pressure difference, $\bar{p}$, is inserted into the equations and we can construct a pressure equation that solves for the pressure at either the top or the bottom of the reservoir. We choose to find the top pressure and we construct the pressure equation for the vertically averaged parameters as it is done in section 2.2.6.

3.4 Height of the Interface given by the Saturation of CO_2

To get rid of the dependence of z in the expression for h, we scale the height of the reservoir so that the height is set to 1.

$$H' = \frac{H}{H} = 1 \tag{3.40}$$

$$h' = \frac{h}{H} \tag{3.41}$$

$$H' - h' = 1 - h' = \frac{H - h}{H} \tag{3.42}$$

Now the vertically averaged CO_2 and brine saturations equal:

$$\hat{S}_c = \frac{1}{H}\int_0^H S_c \mathrm{d}z = \frac{h}{H} \tag{3.43}$$

$$\hat{S}_b = \frac{1}{H}\int_0^H S_b \mathrm{d}z = \frac{H - h}{H} \tag{3.44}$$

$$\hat{S}_c + \hat{S}_b = 1 \tag{3.45}$$

So when the height is scaled to 1 we can use the vertically integrated saturations as expression for the interface height. We can therefore substitute the saturations back into the equations, and then end up with a continuity equation for the vertically averaged saturation.

$$h'(\mathbf{x}, t) = \hat{S}_c(\mathbf{x}, t) \tag{3.46}$$

$$H' - h'(\mathbf{x}, t) = 1 - \hat{S}_c(\mathbf{x}, t) = \hat{S}_b(\mathbf{x}, t) \tag{3.47}$$

From now on we scale the height in all the equations, leaving the height of the scaled interface as the vertically integrated saturation of the CO_2, which we

choose do call S. For the rest of the thesis we refer to the vertically integrated and scaled variables as the 2 dimensional variables, in other words we drop the hat-notation.

3.5 Summary of the Vertically Averaged Formulation

The vertical integration yields a continuity equation in 2 dimensions, integrated horizontal fluxes as functions of the vertical varying pressure and a relation between the pressure in the two phases that enables us to construct a pressure equation and close the mathematicalare model.

- We start out with a physical problem in 3 dimensions.
- By reasonable assumptions and vertical integration we simplify the system to equations of 2 dimensions.
- The vertically averaged saturation describes the vertical dimension.
- The local capillary pressure is substituted by the global vertical pressure difference between the top and the bottom of the reservoir
- A lot of computation time and power is saved and we hopefully get a good approximation of the 3 dimensional flow in the reservoir.
- We refer to the model with the vertical equilibrium assumptions as the VE model, and the model with the structured vertical velocity assumption is referred to as the VSS model

The 2 dimensional model equations we use to simulate the 3 dimensional two-phase flow include the pressure equation:

$$-\nabla \cdot \mathbf{K}\lambda_T \nabla p_c = q - \nabla \cdot \mathbf{K}\lambda_b \nabla \bar{p} \tag{3.48}$$

which provides the pressure needed to calculate the Darcy velocities:

$$\mathbf{v}_c = -\mathbf{K}\lambda_c \nabla p_c, \quad \mathbf{v}_b = -\mathbf{K}\lambda_b \nabla (p_c - \bar{p}). \tag{3.49}$$

The CO_2 Darcy velocity is used to update the saturation equation:

$$\phi \frac{\partial S}{\partial t} + \nabla \cdot \mathbf{v}_c = \frac{q_c}{\rho_c} \tag{3.50}$$

The vertical pressure difference for the model of the vertical equilibrium assumption (VE):

$$\bar{p} = -g\rho_c S - g\rho_b(1-S) \tag{3.51}$$

and the vertical pressure difference for the structured vertical velocity assumption (SVV):

$$\begin{aligned} \bar{p} = \quad & -g\rho_c S + \frac{1}{2\mathbf{K}_z}\left(\mu_c(\mathbf{v}_c \cdot \nabla S + S\phi\frac{\partial S}{\partial t})\right) \\ & -g\rho_b(1-S) + \frac{1}{2\mathbf{K}_z}\left(\mu_b(\mathbf{v}_b \cdot \nabla S + (1-S)\phi\frac{\partial S}{\partial t})\right) \end{aligned} \tag{3.52}$$

Chapter 4

Discretization and Implementation

The numerical solution is calculated by using a finite-volume method. We start with the model from [1] and develop it further. The code is implemented in Matlab and we use many built-in functions of Matlab.

4.1 Grid

The grid used is a regular quadratic grid with equally sized grid cells. The advantage of using a regular grid is that the implementation of the dicretized equations is kept simple.

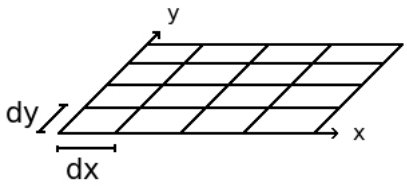

Figure 4.1: Regular quadratic grid

4.2 IMPES

IMPES stands for IMplicit Pressure Explicit Saturation.
The pressure is found implicitly by solving a system of linear equations. The saturation is calculated by a first order explicit Euler method. We choose

the grid size as we please and let a CFL-condition controll the size of the time steps.

4.2.1 Solving the System of Equations

The first step of solving the system is to give the initial and boundary conditions. We will assume that there is no transport of mass over the outer boundary of the reservoir.

$$\mathbf{v} \cdot \mathbf{n} = 0 \text{ on } \partial\Omega$$

where $\mathbf{n}$ is the normal vector pointing out of the reservoir and Ω and $\partial\Omega$ denote the reservoir and the boundary of the reservoir respectively.

Initially the saturation of one of the phases must be given. A typical initial value would be

$$S_c = 0 \text{ in } \Omega,$$

meaning that the reservoir is filled with brine before the injection of CO_2 begins. The following procedure is the usual way of solving the IMPES-method:

1. Give initial conditions
2. Solve the pressure equation (3.48)
3. Calculate vertical pressure difference (3.52) or (3.51)
4. Calculate phase velocities using Darcy's law (3.49)
5. Solve the saturation equation (3.50) and update saturation
6. One time step completed, start over from step 2 using the new values obtained at this time step

The pressure equation is solved using the Two-Point Flux-Approximation(TPFA) scheme. The method uses the information from two neighbouring cells and calculates the flux over the cell interface. The pressure difference between the cells drives the flow and the volumetric fluxes are found by multiplying that pressure difference by the transmissibility of the cells' interface. Transmissibillities are the the total conductivity between two cells, including both the properties of the rock and the phases.

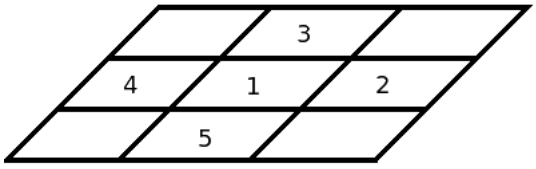

Figure 4.2: 5-cell model

Each cell in the grid has a maximum of 4 neighbouring cells and the sum of the flux over all the interfaces of a cell is equal to the source-or-sink term inside the cell.

$$\sum_{l=2}^{5} v_{1,l} = q_1 \delta_{ij}$$

The CO_2 saturation is updated by summing the CO_2 flux into a cell. To avoid unphysical behaviour in the model we use the upstream value of the saturation parameters. In other words we use the parameters from the cell of which the flow is coming from.

4.3 Vertical Pressure Difference

Calculating the vertical pressure difference in the VE model (equation (3.51)) is a straight forward operation which can be compared with the calculation of the capillary pressure mentioned in section 2.2.3. The vertical pressure difference is a function only of the saturation of CO_2 and the horizontal gradient of the pressure difference can be calculated using the chains rule:

$$\nabla \bar{p}_{\mathrm{VE}} = \frac{\partial \bar{p}_{\mathrm{VE}}}{\partial S} \nabla S = g(\rho_b - \rho_c) \nabla S \tag{4.1}$$

However the vertical pressure difference in the SVV model is dependent on both the saturation, the derivatives of the saturation and the phase velocities. We can not use the same simple chains rule when we want to calculate the gradient of the vertical pressure difference. The vertical pressure difference must therefore first be calculated before we can calculate the horizontal gradient numerically.

4.3.1 Discretizing the Vertical Pressure Difference

Since we wish to use two different methods and compare the two methods to each other, we should try to calculate the two methods as equally as possible.

The pressure equation (3.48) is solved at time step $k+1$:

$$-\nabla \cdot (\mathbf{K}\lambda_T^k \nabla p_{TOP}^{k+1}) = q + \nabla \cdot (\mathbf{K}\lambda_b^k \nabla \bar{p}^k) \tag{4.2}$$

For the VE model the vertical pressure difference is calculated after the each update of the saturation.

$$\bar{p}_{\mathrm{VE}}^k = \bar{p}_{\mathrm{VE}}(S^k) \tag{4.3}$$

If we do the same for the SVV model we face a challenge. The vertical pressure difference in the SVV model depends in addition to the saturation, on the phase velocities. If we use the updated saturation and the phase velocities calculated on the same time step we get an expression that depends phase velocities based on the old saturation:

$$\bar{p}_{\mathrm{SVV}}^k = \bar{p}_{\mathrm{SVV}}(S^k, \mathbf{v}_\alpha(\bar{p}^{k-1})) \tag{4.4}$$

We wish to express the vertical pressure difference as an expression depending on the updated saturations with the matching phase velocities so that

$$\bar{p}_{\mathrm{SVV}}^k = \bar{p}_{\mathrm{SVV}}(S^k, \mathbf{v}_\alpha(\bar{p}^k)) \tag{4.5}$$

We could solve this problem by solving the pressure equation, but to do that we need the vertical pressure difference, which is what we are trying to calculate. In stead we take advantage of the fact that pressure changes less rapidly in time than saturation [6], and we assume that we can use top pressure calculated at the given time step k. Then we just need to insert the updated saturation into the saturation dependent parameters of the phase velocities. However the vertical pressure difference from the previous time step is still in the expression for the vertical pressure difference at the current time step through the brine velocity. The problem is therefore: the brine velocity and the vertical pressure difference are dependent on each other and should be calculated at the same time. The phase velocities are given as:

$$\mathbf{v}_c = -\mathbf{K}\lambda_c \nabla p_{top} \tag{4.6}$$

$$\mathbf{v}_b = -\mathbf{K}\lambda_b \nabla (p_{top} - \bar{p}) \tag{4.7}$$

and the vertical pressure difference is given in equation (3.52). The only change we need to do in the CO_2 velocity is to use the updated saturation. For the brine velocity the vertical pressure term is also changed.

The goal is to calculate the brine velocity at the same time as the vertical pressure difference, to obtain an expression for the vertical pressure difference. Then the vertical pressure difference inserted into the pressure equation at the next time step depend only on parameters calculated at the current time step.

Iterative Calculations

The first method we tried was a straight forward Jacobi iteration.

- Do until convergence:

  - Calculate the phase velocities based on the last calculated saturation and vertical pressure difference

  - Use the calculated phase velocities to calculate the vertical pressure difference

This procedure is in fact a fixed-point iteration for the brine velocity.

$$v_b = f(v_b)$$

Fixed-point iterations have linear convergence and converge only if the initial guessed value is close enough to the real value. For the first time steps the procedure converged but after a while the value of the vertical pressure difference diverged to negative and positive infinity at different locations in the reservoir. To deal with the problem we could have used a different iterative method to speed up the convergence, but in stead we chose to calculate the vertical pressure difference in a different manner.

Simultaneous Calculations

The next method we tried was to avoid calculating the phase velocities and using the definition of the phase velocities in the expression for the vertical pressure difference. We have 2 equations: vertical pressure difference (3.52) and the brine flux equations (4.7), with 2 unknowns. The brine velocity equation only contains the vertical pressure difference as unknown so we insert the equation into the vertical pressure difference expression. The result is a vertical pressure difference equation with only one unknown (vertical pressure difference) which we solve for. This procedure leads to a stable method of calculating the vertical pressure difference.

$$\begin{aligned} \bar{p} = \quad \bar{p}_{\mathrm{VE}} \quad & + \frac{1}{2\mathbf{K}_z}\Big(\mu_w(\mathbf{v}_b \cdot \nabla S) + \mu_c(\mathbf{v}_c \cdot \nabla S)\Big) \\ & + \frac{1}{2\mathbf{K}_z}\left((\mu_w(1-S) + \mu_c S)\phi\frac{\partial S}{\partial t}\right) \end{aligned} \tag{4.8}$$

where

$$\bar{p}_{\mathrm{VE}} = -\rho_b g(1-S) - \rho_c g S. \tag{4.9}$$

Inserting the brine velocity (4.7) and rearranging the terms gives a new expression. First we expand the expression containing brine velocity multiplied by the saturation gradient which gives

$$\mathbf{v}_b \cdot \nabla S = -K\lambda_b \nabla p_{top} \cdot \nabla S + K\lambda_b \nabla \bar{p} \cdot \nabla S \tag{4.10}$$

The last term of the equation above is further expanded and moved to the left side of the equation. Now all terms containing the vertical pressure difference is on the left side.

$$\begin{aligned} &\bar{p} - \frac{\mu_b \lambda_b}{2K_z}\left(K_x \frac{\partial S}{\partial x}\frac{\partial \bar{p}}{\partial x} + K_y \frac{\partial S}{\partial y}\frac{\partial \bar{p}}{\partial y}\right) = \bar{p}_{VE} \\ &-\frac{\mu_c}{2K_z}\left(K\lambda_c \nabla p_{top} \cdot \nabla S\right) + \frac{\mu_b}{2K_z}\left(\mathbf{v}_c \cdot \nabla S\right) + \frac{1}{2K_z}\left(\mu_w(1-S) + \mu_c S\right)\phi\frac{\partial S}{\partial t} \end{aligned} \tag{4.11}$$

We treat the terms $\frac{\partial \bar{p}}{\partial x}$ and $\frac{\partial \bar{p}}{\partial x}$ as a derivation matrix times a vector $\bar{\mathbf{p}}$, and recognise the equation above as a system of linear equations.
If we assume that the reservoir consists of n grid cells then we can rewrite equation (4.11):

$$\left(\mathtt{I} - \frac{\mu_b \lambda_b}{2K_z}(\mathtt{X} + \mathtt{Y})\right)\bar{\mathbf{p}} = \mathbf{b} \tag{4.12}$$

where

- $\mathtt{I}$ is the $(n \times n)$ identity matrix
- $\frac{\partial}{\partial x}$ and $\frac{\partial}{\partial y}$ are two-diagonal $(n \times n)$ derivation matrices
- $\mathtt{X} = K_x \frac{\partial S}{\partial x}\frac{\partial}{\partial x}$ is an $(n \times n)$ matrix
- $\mathtt{Y} = K_y \frac{\partial S}{\partial y}\frac{\partial}{\partial y}$ is an $(n \times n)$ matrix
- Both $\bar{\mathbf{p}}$ and $\mathbf{b}$ are $(n \times 1)$ vectors
- Each entry in the vectors and each row in the matrices correspond to one grid cell

Now $\bar{p}$ is easily found by solving the system of linear equations.

$$\left(\mathtt{I} - \frac{\mu_b \lambda_b}{2K_z}(\mathtt{X}+\mathtt{Y})\right)\bar{\mathbf{p}} = \mathbf{b} \quad \Rightarrow \quad \bar{\mathbf{p}} = \left(\mathtt{I} - \frac{\mu_b \lambda_b}{2K_z}(\mathtt{X}+\mathtt{Y})\right)^{-1}\mathbf{b}$$

The matrix $\left(\mathtt{I} - \frac{\mu_b \lambda_b}{2K_z}(\mathtt{X}+\mathtt{Y})\right)$ has a sparse pattern so the computational cost of solving the system of linear equations is low when using Matlab's built-in functions.
We end up with the result we wanted:

$$\bar{p}^k = \bar{p}(S^k, p^k) \tag{4.13}$$

Now the vertical pressure difference is a function of the updated saturation and we get a more physical correct basis for the solving of the pressure equation at time step k.

4.3.2 Implementing the Vertical Pressure Difference for the SVV Model

We ran the implemented code for various injection rates in a 2D reservoir simulation. Since the model implemented in Matlab is so simple, the IMPES method breaks down at some points in the SVV model. At first it seemed that the code broke down when we considered low injection rates. At low enough injection rates it seemed that the flow caused by the vertical pressure difference was grater than the flow from the global, horizontal pressure difference. The results of this were unphysical solutions and oscillations in the saturation of CO_2. In order to understand the unphysical behaviour in the simulations we set up a 1-dimensional test-example.

1D Reservoir Test-Example

We consider a reservoir divided into 3 grid cells initially filled with brine. In the first cell(see figure 4.3) there is a well injecting CO_2 and in the third cell a well is producing whatever reaches the well. The volume injected into cell 1 is equal to the volume produced from cell 3.

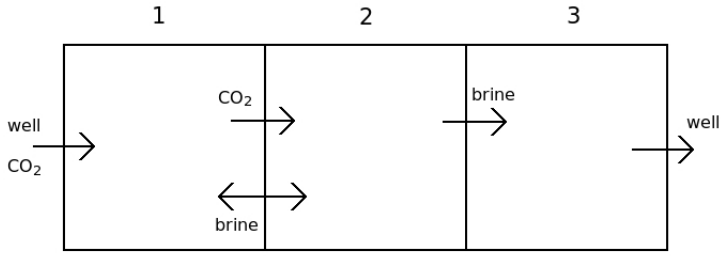

Figure 4.3: 3 block example

Now we can study the flow over the cell-interface between cell 1 and 2. The problem we encountered at the low injection rates can be described in the test-example.

A small amount of CO_2 is injected into cell 1 displacing brine at the first time step. The brine flows over the cell-interface and into the second cell. At the second time step the CO_2 flows into the second cell because of the vertical pressure difference. But then at the same time the brine flows in the opposite direction and back into the first cell. The saturation profile will then oscillate as the brine flows back and forth over the cell interface. The resultant brine flow velocity changes with the injection rate and figure 4.4 shows a sketch of what that may look like.

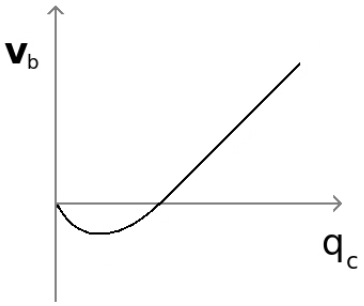

Figure 4.4: Resultant brine velocity between cell 1 and 2 as a function of the injection rate of CO_2

The goal of looking at the test-example is to find the injection rate at which the brine flow velocity is equal to zero. In other words, to find the

injection rate of CO_2 that balances the flow of brine caused by the vertical pressure difference.

Restrictions on the grid size

In the following we return to the vertically averaged model with respect to the interface h. We assume that the injection rate q of CO_2 is small and that the time step $\Delta t << 1$. After the injection during the first time step the height of the interface in the first cell becomes:

$$h_1^1 = \frac{q_c \Delta t}{\phi \Delta x} \tag{4.14}$$

The saturation of CO_2 in the second cell is $h_2^1 = 0$.

The value of $h_1^1 << 1$, so the part of the vertical pressure difference equation (3.52) that is multiplied by h_1^1 vanishes. The brine flow velocity is equal to zero so the only part left of the vertical pressure difference is

$$\bar{p}_{\text{SVV}} = -g\rho_b H + H\frac{\mu_b}{K_z}\left(\phi\frac{\partial h}{\partial t}\right) = -g\rho_b H + H\frac{\mu_b}{K_z}\left(\phi\frac{h_1^1 - h_0^1}{\Delta t}\right). \tag{4.15}$$

We insert the expression for the saturation of cell 1 and the vertical pressure difference expression in the first cell is then reduced to:

$$\bar{p} = p_c - p_b = -g\rho_b H + \frac{\mu_b}{2K_z}(H\frac{q}{\Delta x}) \tag{4.16}$$

Next we use Darcy's law between cell 1 and 2 to find an expression for the pressure in the phases. The CO_2 pressure in the second cell is zero since no CO_2 has reached that cell. The CO_2 pressure in the first cell is then:

$$p_c = \frac{v_c \mu_c \Delta x}{K} + p_i \tag{4.17}$$

where p_i is the initial top pressure in the reservoir. Since the brine flow velocity is zero, by assumption the brine pressure is equal for the two first cells. The brine pressure is therefore equal to the initial reservoir top pressure plus the hydrostatic pressure(Vertical Equilibrium):

$$p_b = p_i + g\rho_b H \tag{4.18}$$

Since CO_2 is the only phase flowing in this test-example we assume that the flow velocity of CO_2 is equal to the injection rate:

$$v_c = \frac{q_c}{\Delta x} \tag{4.19}$$

Now we insert the two pressure expressions ((4.17), (4.18)) into the vertical pressure difference expression above ((4.16)) and we end up with:

$$\begin{aligned} &\frac{\mu_c}{K_x} q_c = \frac{\mu_b H}{2K_z \Delta x} q_c \quad \Rightarrow \\ &\left(\frac{\mu_c \Delta x}{K_x} - \frac{\mu_b H}{2K_z} \right) q_c = 0 \end{aligned} \tag{4.20}$$

The idea of the test-example was to find the injection rate q_c where the brine velocity is equal to zero. From (4.20) we get the trivial solution: $v_b = 0$ when $q_c = 0$. There is no flow in the reservoir when nothing is injected.

However equation (4.20) also gives us another result:

$$\Delta x = \frac{1}{2} \frac{\mu_b K_x}{\mu_c K_z} H = \gamma H \tag{4.21}$$

This relation is interesting since it tells us that the brine does not flow if we choose Δx as given above. For $\Delta x < \gamma H$ the brine flows in the negative direction and opposite for $\Delta x > \gamma H$.

We can not let $\Delta x \to 0$ since this gives unstable solutions. What we thought was the reason for the unstable solution turned out to give restrictions on how we choose the size of the grid cells.

We have already chosen to scale the height of the reservoir to 1, so the unit of the length in the horizontal direction is therefore given in *reservoir heights*, H.

However we may intuitively understand the restrictions given for the grid size. We are dealing with parameters that depend on the reservoir height H. The *pseudo 3D-size* of each grid cell is therefore (Δx, Δy, H). If we choose Δx or Δy or both much smaller than the pseudo $\Delta z = H$, we get grid cells shaped as columns since there is no partition of the vertical length. It may be understandable that the simulation breaks down when the parameters of the vertical pressure difference in the column-grid cells depend on the full length scale vertically but a partition of the horizontal scale.

Then again, the restriction does not apply to the vertical equilibrium solution. The reason for this may be that the vertical equilibrium part of the vertical pressure difference is implemented in the same way as capillary pressure would have been. The saturation in the grid cells represents the height of the interface but it also represents the saturation in the horizontal grid cell of the size (Δx, Δy). The vertically averaged model with phases in vertical equilibrium can be viewed as a horizontal reservoir where the capillary pressure is accounted for.

We know from [15] that the effect of the vertical velocity part of the vertical pressure difference is greatest in the areas close to a well. The difference between the VE model and the SVV model is biggest within a region of approximately 1.5 H around the well. In the chapter on simulations we will use parameters from a typical aquifer in North America suited for CO_2 storage. The parameters give the restriction $\Delta x > 0.4H$. Therefore we can only divide the most interesting area around a well into two grid cells. This is not very promising, but we still which to use the model and look at some examples where it is applicable.

Numerical Reason for Restrictions

We look at the vertical pressure difference in one dimension and we want to analyse the effect the different terms in the expression have on the value of the vertical pressure difference. The expression is dominated by two terms:

$$\frac{\partial S}{\partial x} v_x, \qquad \frac{\partial S}{\partial t}. \tag{4.22}$$

Since we inject CO_2 and thereby increase the saturation, the time derivative of saturation must have a positive value. The space derivative of saturation and the flux-velocity on the other hand have opposite signs. If we inject CO_2 at x=0 the flow will go in positive x-direction giving the flux-velocity a positive value. The CO_2 saturation is then greatest at x=0 and decreases with increasing x-values and the value of the derivative of the saturation is therefore negative. If we were to inject CO_2 at x>0 and get flow in negative x-direction the derivative of the saturation would be positive. That leads to the conclusion that the sign of $\frac{\partial S}{\partial x} v_x$ is always negative for these initial conditions.

We consider the one dimensional reservoir. We have an injection well in one end and a production well in the other end of the reservoir. After the

first time step some amount of CO_2 is injected. The amount of CO_2 injected is dependent on the injection rate of the injector and the length of the time step. Though the total volume of injected CO_2 is the same for all sizes of the grid we choose, the size of the grid cells is important in calculating the non-linear as well as the linear capillary pressure. After the first time step the saturation in the first cell, the well cell, is equal to the injected volume divided by the total volume of the cell.

$$S_1(t = \Delta t) = \frac{q}{\Delta x \Delta y} \Delta t \tag{4.23}$$

where Δy is a constant in the one dimensional case. It is now easy to calculate the derivatives in the first cell. The saturation in the neighbouring cell must be equal to zero if the the length of the time step is small enough. Because we use a finite volume method, the volume flux over the cell boundary is balanced by the source. That means that the the volume flux between the first and the second cell must equal the injected volume. The flux-velocity in each cell is equal to the volume flux divided by the width of the cell. Further the space derivative is equal to the difference between the saturation in the second and the first cell divided by the distance between the two cell centres.

$$v_1(t = \Delta t) = \frac{q}{\Delta y} \qquad \frac{\partial S_1}{\partial x}(t = \Delta t) = -\frac{q}{\Delta x \Delta y} \Delta t \frac{1}{\Delta x} \tag{4.24}$$

The time derivative of the saturation is equal to the saturation at the given time step minus the saturation at the previous time step divided by the length of the time step.

$$\frac{\partial S_1}{\partial t}(t = \Delta t) = \frac{q}{\Delta x} \Delta t \frac{1}{\Delta t} = \frac{q}{\Delta x \Delta y} \tag{4.25}$$

The vertical pressure difference is clearly dependent on the grid size. After the first time step the expression is dominated by:

$$\frac{\partial S}{\partial x} v \sim \frac{q \Delta t}{(\Delta x)^2 (\Delta y)^2} \qquad \frac{\partial S}{\partial t} \sim \frac{q}{\Delta x \Delta y} \tag{4.26}$$

Unfortunately the vertical pressure difference expression does not converge when we decrease the size of Δx and Δt. If we set $\Delta t = 1$ and vary the size of Δx we see that for $\Delta x > 1$ the term $\dfrac{\partial S}{\partial t}$ dominates the expression while the term $\dfrac{\partial S}{\partial t} v$ dominate when $\Delta x < 1$.

Now if we fix Δx and vary Δt we see that only the term $\dfrac{\partial S}{\partial x} v$ will be effected by that.

When we choose a fine grid, the numerical value of the vertical pressure difference overcomes the global horizontal pressure difference due to the numerical method we use. In order for the IMPES model suggested over to run smoothly, we have to base the calculations on a grid with sizes as given in equation (4.21).

4.3.3 Expected Importance of the Vertical Pressure Difference

From the equations we have that the flow is driven by the global pressure and the vertical pressure difference. The flow rate is proportional to the horizontal gradient of the global pressure and the horizontal gradient of the vertical pressure difference. As long as we inject a fluid as pressure support into the reservoir we are producing from, the total pressure is not changed much, thus the total velocity does not change that much. The vertical pressure difference may change relatively more than the global pressure, but when can we expect the vertical pressure difference to be of importance?

The linear part of expression (3.52) only depends on the saturation and causes the phases to flow in at a velocity proportional to the gradient of the saturation. So when ∇S has its biggest absolute value the linear part is at its largest in absolute value. ∇S is biggest when two neighbouring cells are fully saturated by opposite phases. In the numerical examples we will return to a special case of this example.

As we showed above, the vertical velocity part of the vertical pressure difference depends on the horizontal phase velocities and the derivatives of the saturation. We expect that the value of the vertical pressure difference is biggest where the velocities are big.

The time derivative of the saturation denotes the change of saturation in grid cell. For a homogeneous reservoir the sum of the change is constant for each time step.

$$\sum_{i=1}^{n} \frac{\partial S_i}{\partial t} = C \tag{4.27}$$

In the first time steps the grid cells closest to an injection well are the only grid cells that contain CO_2. As the CO_2 spreads throughout the reservoir the term $\dfrac{\partial S}{\partial t}$ is distributed over a larger area and more cells. This term is

therefore largest after the first time step and is smeared out and follows the saturation front as the CO_2 flows away from the well. Obviously the value of this term is equal to zero in the cells where the saturation is constant.

Chapter 5

Simulations

In the simulation examples we use the same parameters as Nordbotten and Celia [15]. The properties of the CO_2 and brine are calculated from pressure, temperature and salinities that are typical for CO_2 injection in North America. The aquifer is located at 3000 m below the surface, the surface temperature is 10°C and a geothermal gradient of 25°C per kilometer. The amount of salt and minerals dissolved in the water is about 0.2 mole fraction.

Parameter	Value
Aquifer thickness H	15 m
CO_2 density ρ_c	733 kg/m^3
Brine density ρ_b	1099 kg/m^3
CO_2 viscosity μ_c	0.0611 mPa s
Brine viscosity μ_b	0.511 mPa s
Horizontal permeability $\mathbf{K}$	20 mD
Vertical permeability $\mathbf{K}_z$	200 mD
Gravitational constant g	9.81 m/s^2

5.1 Lock-Exchange with Gravity-Driven Flow

The Lock-Exchange problem for gravity-driven flow is a good test case to evaluate the vertically averaged models [13]. In this problem we consider the two phases initially separated by a sharp vertical interface, there are no sources or sinks in the reservoir and no flow over the outer boundary. The total volume of CO_2 is therefore constant at all times. The gravity induces the flow, and as $t \to \infty$ the phases reach a steady state where the CO_2 phase

totally overrides the brine-phase. In an 'unphysical' reservoir the vertical cut of the process would look like the sketch in picture 5.1.

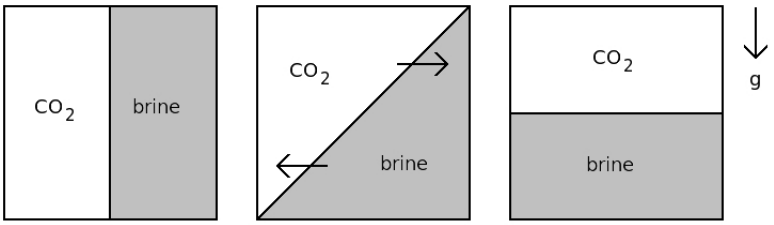

Figure 5.1: Gravity-driven Flow

At $t = 0$ there is no flow in the reservoir, but the phases start to flow because of the density difference between the phases. For the VE model the horizontal gradient of the vertically averaged pressure has its maximum value on the interface between the phases before the phases start to flow. The vertically averaged velocities should therefore, at least for the VE model, be largest in the beginning of the simulation and decrease in time.

5.1.1 Lock-Exchange Examples

We consider a reservoir with horizontal lengths of 150*150 meters. It is worth noting that the grid size restriction also alplies to the simulations where there are no injections. The flow of brine in negative direction however, is not a problem. Figure 5.2 shows how the interface is moving in time after different time steps. In figure 5.2(a) we zoom in on the vertical interface between the phases, while figure 5.2(b) shows the full length of the small reservoir. Here we see that the interface heights in the two different models are different from each other. Figure 5.3(a) shows the maximum difference between the two models after 28 hours. The result from SVV is then about 1/2 m above the from the VE model on the top of the interface, and 1/2 m below on the bottom of the interface. The interface height changes less rapidly in the SVV model than in the VE model until 28 hours. After that the SVV model 'catches up' with the VE model, and from 20 days and until the steady state is reached, the interface height in the two models are close to being equal.

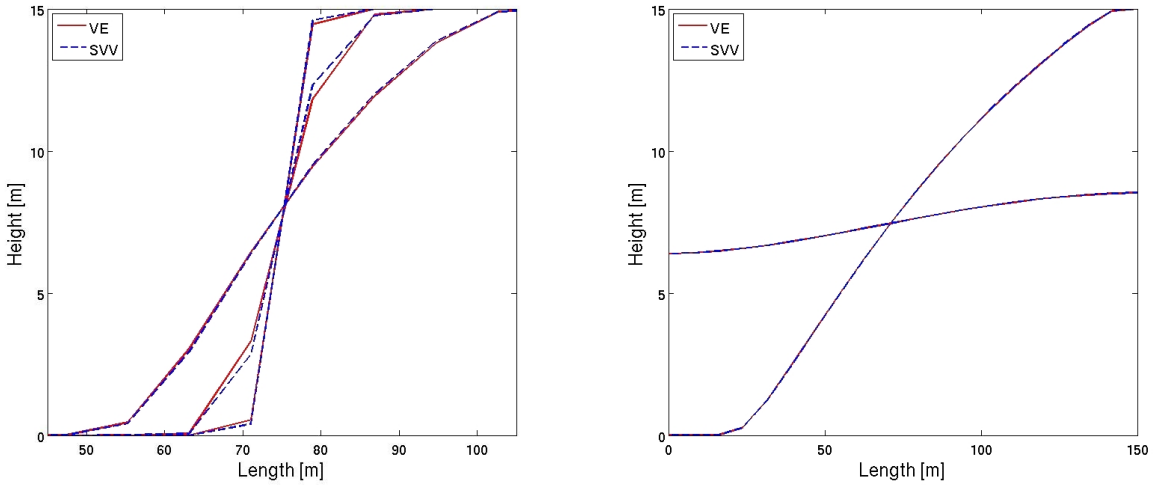

(a) (b)

Figure 5.2: Lock-exchange with gravity-driven flow. (a): Interface after 3 hours, 28 hours and 12 days. (b): Interface after 115 days and 1150 days.

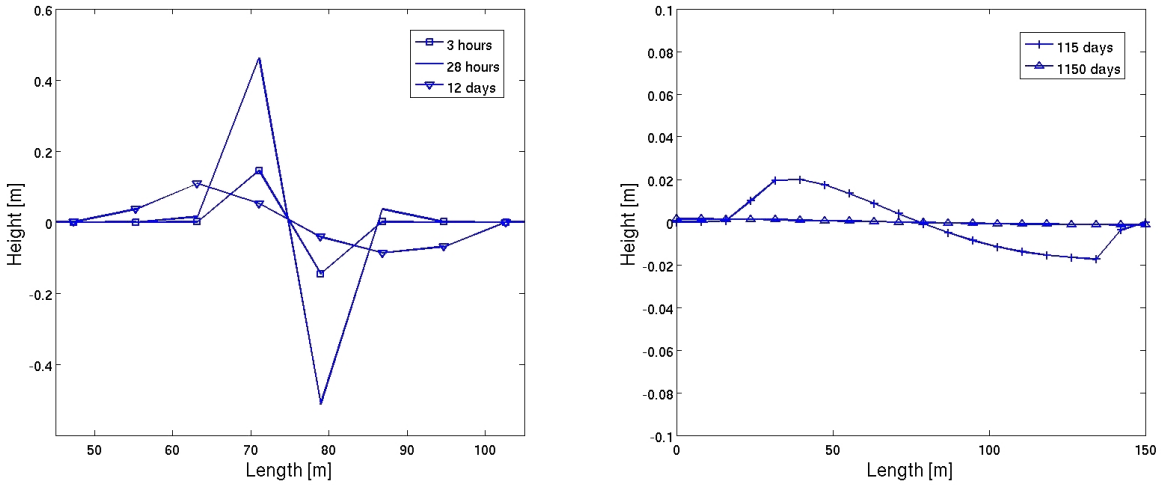

(a) (b)

Figure 5.3: Difference in the height of the interface between the two methods for the lock-exchange problem. (a): Difference after 3 hours, 28 hours and 12 days. (b): Difference after 115 days and 1150 days.

While the difference in interface height is close to being symmetric about the initial vertical interface for the first time steps, the vertical pressure difference is not. Figure 5.4(a) shows the vertical pressure difference of the models in the first time intervals, and we see that the SVV model gives lower pressure difference than the VE model in the part of the reservoir initially filled with brine. The reason why this is not seen on the CO_2 side of the reservoir is because of the viscosity and velocity of CO_2. In both models the brine flow on the brine side has greater magnitude than the CO_2 flow on the CO_2 side for the first time steps. Numerically this is so because the horizontal brine flow velocity is calculated based on the horizontal pressure difference on the bottom, which is bigger than the horizontal pressure difference on the top of the reservoir. As the phases flow in opposite directions horizontally at the interface, they will also flow in opposite directions vertically. In this lock-exchange example the brine flows downward and the CO_2 flows upward at the interface. The downward brine flow causes the pressure difference to drop on the brine side of the interface. Even if the vertical CO_2 velocity had been equal in magnitude to the brine velocity, we would still not see the same effect on the vertical pressure difference. This is due to the viscosity of the CO_2, which is 8 times smaller than the viscosity of the brine at the given conditions. In the vertical pressure difference expression for the SVV model the vertical phase velocities are multiplied by the viscosity of the phase, but because of the lower viscosity of the CO_2 phase, the vertical pressure difference is not increased as much on the CO_2 side of the interface.

The pressure drop on the brine side causes the horizontal pressure gradient to be smaller across the interface. Both phases will therefore flow at a lower velocity, and that is why we see that the interface changes slower in the SVV model. Another observation is that the CO_2 flows faster over the brine than the brine flows under the CO_2. This is because of the viscosity of the two phases.

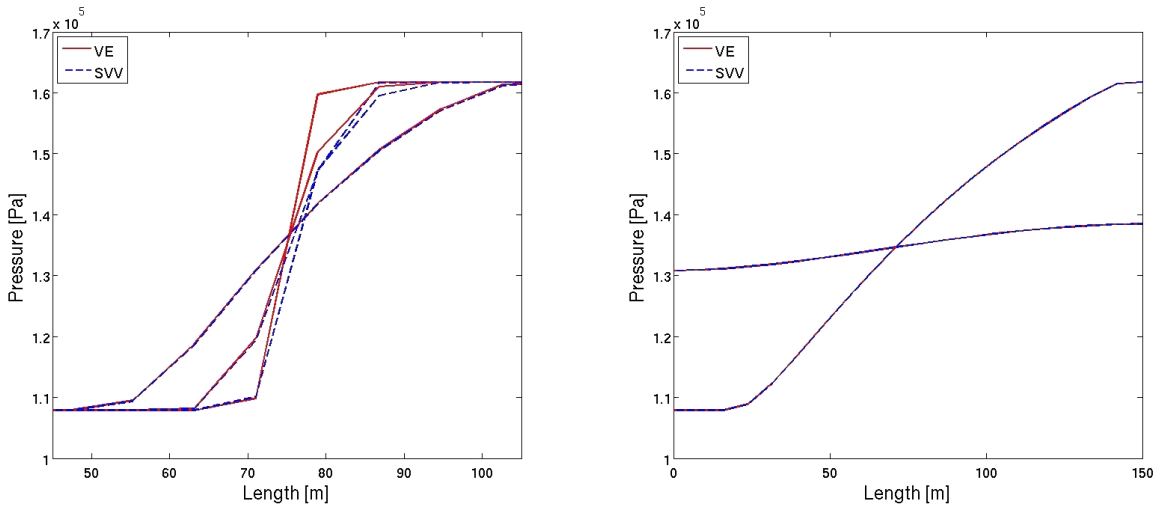

(a) (b)

Figure 5.4: Vertical pressure difference for the lock-exchange problem.(a): 3 hours, 28 hours and 12 days. (b): 115 days and 1150 days.

We see that the vertical pressure difference as well as the interface height in the SVV model converge to the results given by the VE model as time goes.

5.2 Injection of CO_2 into an Aquifer

To test the implemented code when considering an injection problem, we use a standard test reservoir setup with two wells and no flow over the outer boundary.

5.2.1 Quarter-five-spot

Quarter-five-spot is a common test case for two-phase flow simulators. As shown in figure 5.5 we consider one quarter of a five-well problem. We choose to study the upper right quarter of the square and we get a reservoir with two wells, an injector in the lower left corner and a producer in the upper right corner.

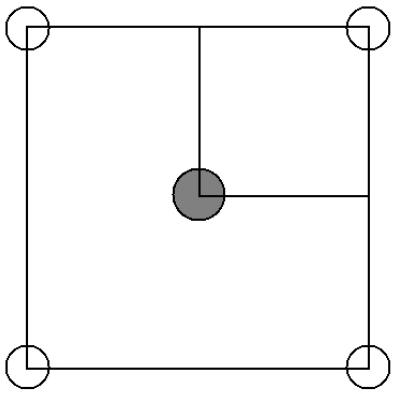

Figure 5.5: Five well problem where the grey circle is an injector and the white circles are production wells

As the injection starts, CO_2 displaces the brine and spreads out through the reservoir (see figure 5.6). Unfortunately it is hard to see the differences between the results of the two methods we are comparing when we look at the full 2 dimensional reservoir. For visualisation purposes we will therefore study the diagonal of the reservoir, going from the injector to the producer. We ran a test simulation of the VE model on a heterogeneous reservoir, and plotted the CO_2 saturation for both the full reservoir and the diagonal. The saturation represents the height of the interface and the horizontal length is scaled by a factor $1/\sqrt{2}$.

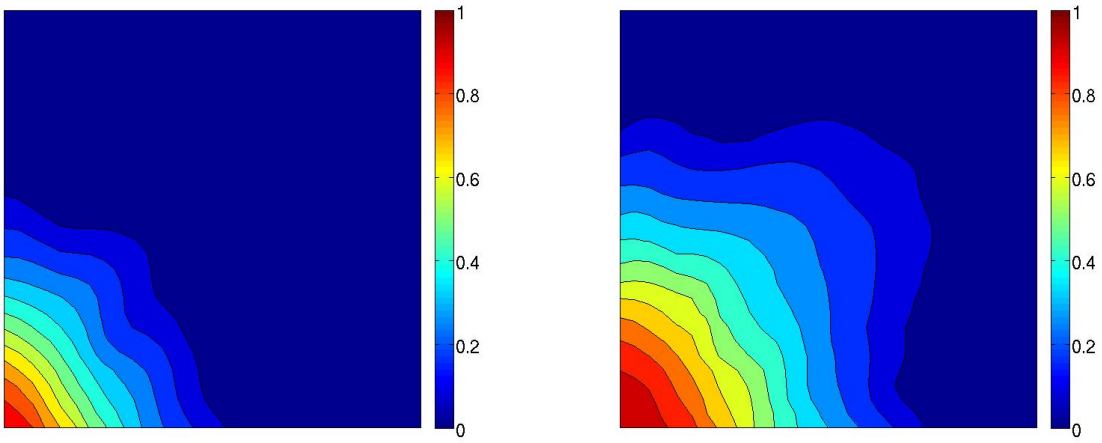

(a) (b)

Figure 5.6: Quarter-five-spot at different time steps in a dimensionless heterogeneous porous media.

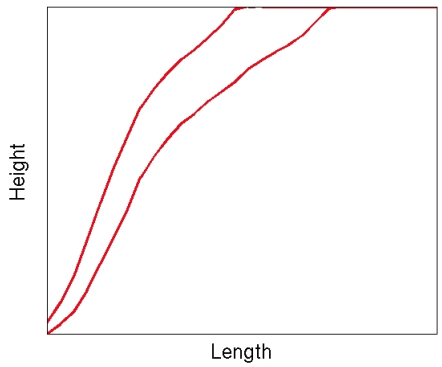

Figure 5.7: Dimensionless reservoir where the upper line corresponds to the diagonal of figure 5.6(a) and the lower line to figure 5.6(b)

The following simulation examples are done in homogeneous quarter-five-spot reservoirs, but we have limited the figures to the diagonal values of the reservoir.

5.2.2 Injection Examples

For injection problems we know that the differences between the model for vertical equilibrium assumption and for the structured vertical velocity assumption is biggest close to the injection well where the vertical velocities tend to be biggest [16]. But the restrictions given for the grid size in equation (4.21) limits the resolution in small areas. Still we first choose to look at the near-well effects before we look at a larger reservoir.

Near-Well Example

We start with a domain of horizontal dimension (150 m * 150 m) where the permeability and porosity are kept constant and as given in table above. We want to study how the result from the two models behave under different injection rates. Intuitively, based on the we can predict that the vertical velocity at the interface will be small when the horizontal velocities are small and bigger when the horizontal velocities are bigger. But we do not know if the vertical velocities are of importance relative to the horizontal flow. So we ran four different simulations where we injected the same volume of CO_2 into the reservoir for all four simulations, and multiplied the injection rate by a factor 10 for each simulation. We started with an injection rate of 1.2 m^3/day and ended with an injection rate of 1200 m^3/day. A sketch of the set up of the injection problem can be seen in figure 3.1.

We see that at the lowest injection rate a plume is formed in the top of the reservoir and the interface between the phases is not very steep. At the higher rates the interface is steeper and the CO_2 has not flowed as far as for the low rate. The difference in the height of the interface between the results of the two models is very small for all the rates, but it increases with increasing rates. The biggest difference is less than 10 cm, which is less than 1% of the reservoir height.
The vertical pressure difference however changes more for the different injection rates. For the three lowest rates (figure 5.9(a)) the vertical pressure differences in the SVV model are nearly identical to the static pressure difference(VE), but for the highest rate (1200 m^3/day) the difference is bigger (figure 5.9(b)). The difference between the models is at most approximately 5%.

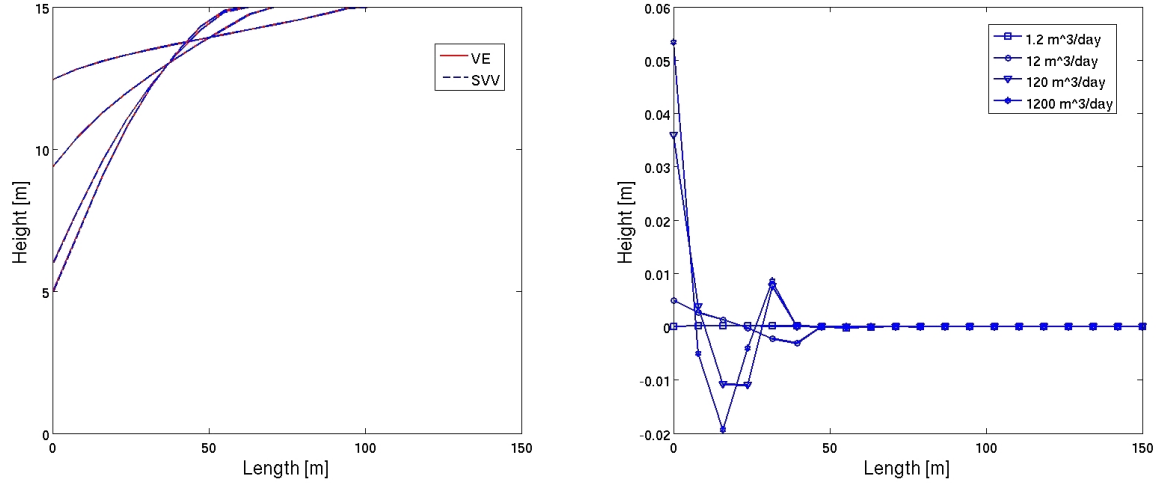

(a) (b)

Figure 5.8: Injection of CO_2 at rates 1.2, 12, 120 and 1200 m^3/day. (a): Interface height. (b): Difference in the interface height between SVV model and VE model.

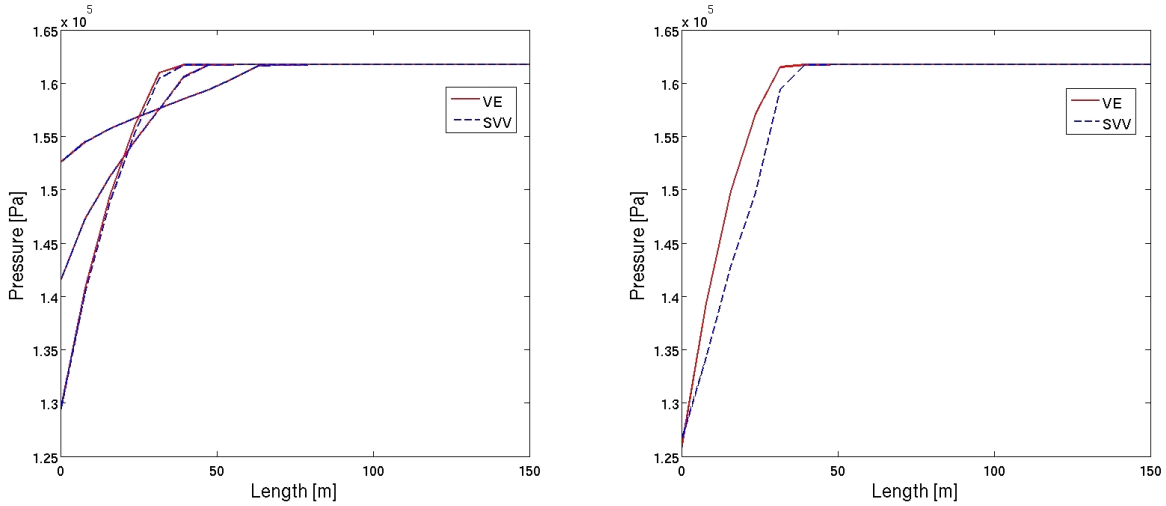

(a) (b)

Figure 5.9: Vertical pressure difference during injection of CO_2. (a): Injection rates: 1.2, 12 and 120 m^3/day. (b): Injection rate: 1200 m^3/day.

Figure 5.9(b) shows that the pressure difference is big so we want to run

a new simulation with the injection rate 1200 m^3/day and plot the interface height and pressure difference at shorter time intervals. Figure 5.10(a) shows a zoom of the interface height from the two models, and figure 5.10(b) shows the vertical pressure difference at the same time steps. When we shorten the time intervals for plotting, we see that the SVV model gives an entirely new solution that we missed when we only looked at longer time intervals. The first line is after only 20 minutes of injection and we see on the pressure plot that the vertical pressure difference is negative meaning that the pressure at the top of the formation is bigger than the pressure at the bottom. If we look at the vertical pressure difference equation for the SVV model (3.52) we see that the vertical velocities at the interface near the well must have negative value in other words, the phases flow upward at the well.

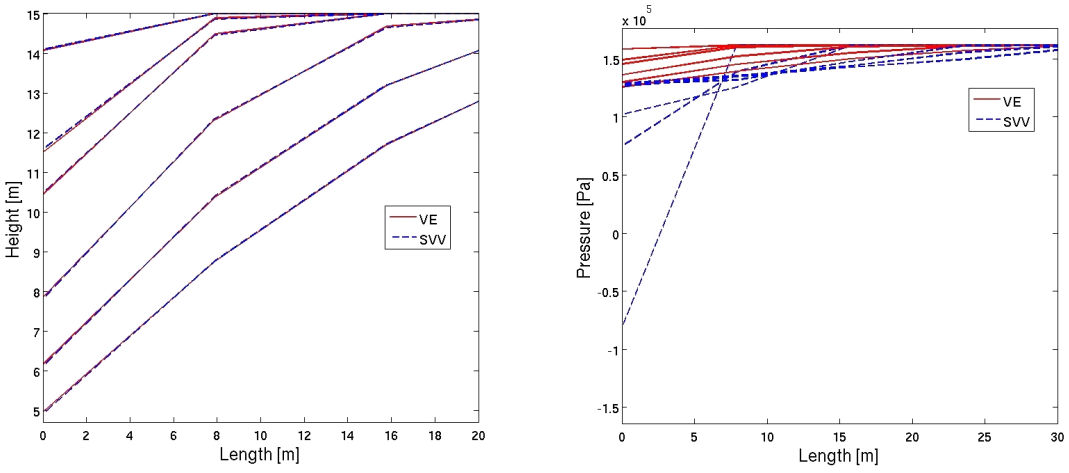

(a) (b)

Figure 5.10: Injection rate 1200 m^3/day(a): Interface height at different time steps. (b): Vertical pressure difference at different time steps.

We also see that the vertical pressure difference from the SVV model closes in on the solution from the VE model. The interface height in the SVV model moves toward the interface from the VE model as we saw in figure 5.8(a).

We tried the same with the other injection rates but found that the biggest difference was for the injection rate of 1200 m^3/day.

If we could have chosen a finer grid we may have seen the effects of the

vertical velocities. Since there is no restriction for the VE model we ran the simulation on both two, three and fours times as fine grids for the injection rate of 1200 m^3/day. The result was a much steeper interface and almost no brine left in the areas closest to the well (see figure 5.11). A steep interface coupled with high horizontal velocities would most likely result in high vertical velocities at the interface. Unfortunately we were not able to study this since the implemented code breaks down in such cases.

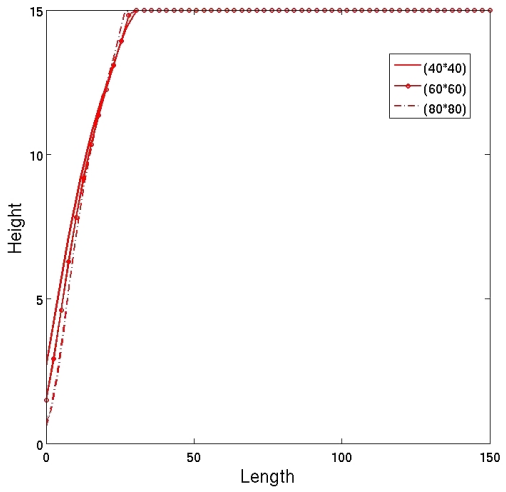

Figure 5.11: VE-simulations of CO_2 injection of 1200 m^3/day with a grid 2, 3 and 4 times finer than in figure 5.8(a)

We also ran a test problem with an injection rate of 12000 m^3/day just to see how the results from the models behave. In general, such an injection rate would most likely cause the pressure in the reservoir to exceed the fracture pressure, and the formation would therefore no longer be suited for CO_2 storage. The maximum allowable injection rate for CO_2 storage is decided based on the fracture pressure of the reservoir, which in turn is based on the properties of the porous rock, such as porosity, permeability and available volume. The Pika aquifer in the Alberta Basin in Canada has a height of 14 m and an intrinsic permeability of 16 mD and the maximum inject rate is 2246 m^3/day [5]. We can compare this aquifer to the simulations done above, where we see that already at an injection rate of 1200 m^3/day, about half of the maximum for the Pika aquifer, the vertical velocities seem to be important near the well.

For the injection rate of 12000 m^3/day the interface height and the differ-

ence in interface height between the solution of the two models are close to identical to the case with an injection rate of 1200m^3/day. But the vertical pressure difference from the SVV model turned out to be only half the vertical pressure difference from the VE model.

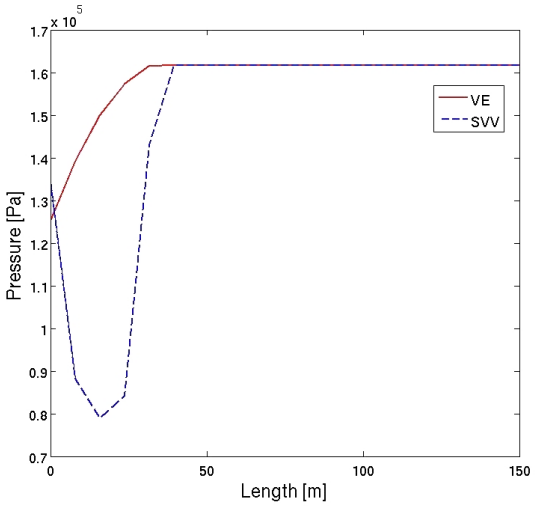

Figure 5.12: Vertical pressure difference at injection rate of 12000 m^3/day.

Higher horizontal velocity gives higher vertical velocity but no significantly change of the interface. For the slow flowing case of the lock-exchange we see that the vertical velocities are a much bigger factor when it comes to the height and shape of the interface 5.2(a). Even though the vertical velocities may be big, the effect on the interface is not big due to the fact that the horizontal velocities are bigger in magnitude.

Smooth Interface away from a Well

The last simulation we present is CO_2 injection into the Pika aquifer at constant maximum rate (2246 m^3/day) in 50 years. We found that there are no significant differences in the interface height nor the pressure differences at any time during the process. Therefore we only show the figure of the interface height 5.13.

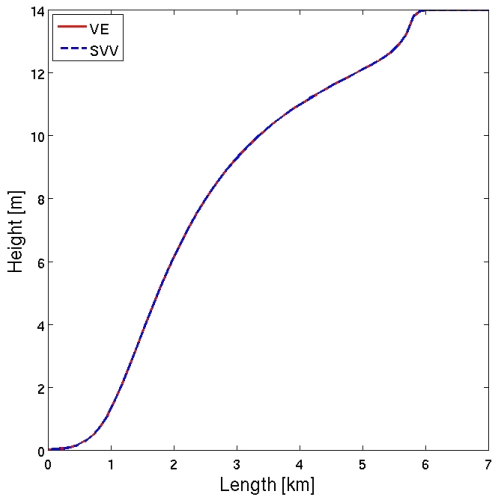

Figure 5.13: 50 years of injection into a reservoir with properties equal to the Pika aquifer.

For grid cells of sizes much larger than the interface height and for flow far away from the well, the SVV models gives the same result as the VE model, as shown in the figure above.

5.3 Computational Time

The computational time for the two models is dependent on a couple of factors. The number of time steps is obviously important, and for high flow velocities or rapid changes in the saturation, the CFL-condition divides the given length of the time step into smaller steps. But these factors apply in equally to both models. The biggest factor when it comes to computational time is the number of grid cells the reservoir is divided into. The time consuming part of the calculations in the SVV model is the implicit calculation of the vertical pressure difference mentioned in section 4.3.1. On each time step four matrix-matrix multiplications and one solving of a linear system are

done in addition to the implicit solving of the global pressure. If the reservoir is divided into n grid cells then the matrices are of size $(n \times n)$. Even though we have used functions available in Matlab to speed up the calculations, this part takes a lot of time.

The simulations are done on a standard desktop computer and the computational time for an arbitrary simulation using different grid sizes is shown in figure 5.14. We see that the computational time needed by the SVV model increases exponentially while the VE model has almost linear growth.

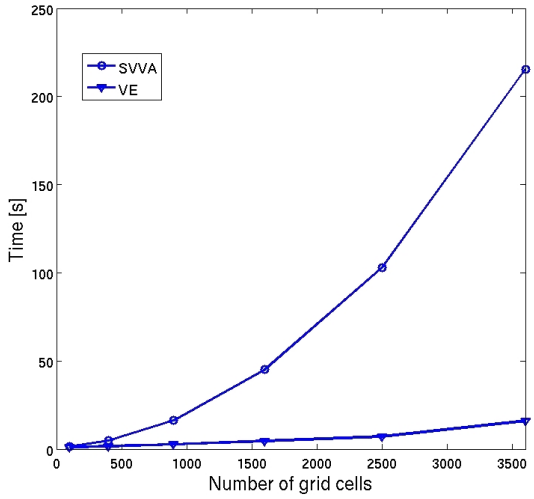

Figure 5.14: Computational time at different grid sizes for the two models when 100 time steps are calculated.

Chapter 6

Summary and Discussion

We have derived and implemented a 2 dimensional vertically averaged two-phase flow model with two different approaches regarding the flow in vertical direction. The model where vertical equilibrium (VE) is assumed, meaning that the phases in the reservoir only flow horizontally, runs smoothly for any grid size and injection rate. In the model of the structured vertical velocity assumption (SVV), where we allow for vertical flow, there are limitations when we use the discretization presented. The resolution of the grid we may use in this method seems to be determined by the height of the reservoir, and the implemented code breaks down when the given restrictions are not met.

We showed that the different methods produced different results in the example of lock-exchange with gravity driven flow. The SVV model gave an interface solution that in the first hours of the simulation changed less rapidly than the solution from the VE model. We also showed that both the vertical pressure difference and the interface solution from the SVV model converged toward the solutions given by the VE model after about 20 days in the simulation.

For the injection examples in the near-well domain we showed that the two models provide the same solution after some time of injection. The vertical velocities were most important in the first time steps of injection near the well, and the magnitude of the vertical flow decreased as more CO_2 was injected. We showed that at unphysically large injection rates the vertical velocity was large but it did not change the shape and height of the interface relative to the interface calculated when vertical equilibrium was assumed. By comparing the injection and the lock-exchange problems we showed that the vertical flow is more important in reservoirs with low horizontal velocities

than in reservoirs with high velocities.

It is important to consider vertical flow in situations where the horizontal velocity is small and the density difference between the flowing phases is big. Vertical flow should also be accounted for when studying flow around wells. It would most likely be an advantage to use a model that can simulate flow in fine grids near a well. The SVV model we have created is not sufficiently good enough to run on near-well problems and the VE model does not even consider the vertical flow. We can therefore conclude that none of the models should be used in close near-well simulations. However the models derived in this thesis can be applied in other simulations. If a simulation is done to calculate the pressure in a reservoir, in for instance risk assessments with focus on leakage through abandoned wells, the vertical pressure variation is important. The two models provide different results on the vertical pressure and we can not say which one does it better. But the structured vertical velocity model has less assumption in the definition of the model, so we would expect it to give a physically more correct answer.

The motivation for the vertical averaging was to be able to simulate large reservoirs where CO_2 is injected for storing purposes. If we run a simulation where the only concern is the interface and how the interface changes during a large scale injection problem, either of the two models can be used since they give the same result, though the vertical equilibrium model would be preferable due to the computational time. The assumption of vertical equilibrium seems to be a good assumption when simulating flow of two phases with high density difference in a large but thin and horizontal reservoir, given that the phases are sufficiently far away from any wells.

References

[1] J. E. Aarnes, T. Gimse, and K.-A. Lie. *Geometrical Modeling, Numerical Simulation, and Optimization: Industrial Mathematics at SINTEF.* Springer Verlag, 2007.

[2] US Environmental Protection Agency. www.epa.gov/climatechange/effects, 2008.

[3] J. Bear. *Dynamics of fluids in Porous Media.* American Elsevier Publishing Company, Inc, 1972.

[4] M. A. Celia. Geological storage as a carbon mitigation option. NGWA Darcy lecture 2008, 2008.

[5] M. A Celia, J. M. Nordbotten, S. Bachu, M. Dobossy, and B. Court. Risk of leakage versus depth of injection in geological storage. *Energy Procedia*, 2008.

[6] Z. Chen, G. Haun, and B. Li. An improved impes method for two-phase flow in porous media. *Transport in Porous Media*, 54:361–376, 2004.

[7] H. Class et al. A benchmark-study on problems related to CO_2 storage in geologic formations. *Computational Geosciences*, 2008. Submitted.

[8] S. E. Gasda, M. A. Celia, and J. M. Nordbotten. Upslope plume migration and implications for geological co2 sequestration in deep, saline aquifers. *The IES Journal Part A: Civil and Structural Engineering*, 2008.

[9] S. E. Gasda, J. M. Nordbotten, and M. A. Celia. Vertical equilibrium with sub-scale analytical methods for geological CO_2 sequestration. *Computiational Geosciences*, 2008. Submitted.

[10] M. A. Hesse, H. A. Tchelepi, B. J. Cantwell, and F. M. Orr Jr. Gravity currents in horizontal porous layers: Transition from early to late self-similarity. *Journal of Fluid Mechanics*, pages 363–383, 2007.

[11] P.K. Kundu and I.M. Cohen. *Fluid Mechanics.* Academic Press, Inc., 2004. ISBN-0-12-178253-0.

[12] L.W. Lake. *Enhanced Oil Recovery*. Prentice Hall, 1989.

[13] I. Lunati and P. Jenny. Multiscale finite-volume method for density-driven flow in porous media. *Computational Geosciences*, 12:337–350, 2008.

[14] A. Neftel, E. Moor, H. Oeschger, and Stauffer B. Evidence from polar ice cores for the increase in atmospheric CO_2 in the past two centuries. *Nature*, 315:45–47, 1985.

[15] J. M. Nordbotten and M. A. Celia. An improved analytical solution for interface upconing around a well. *Water Resources Research*, 42, 2006.

[16] J. M. Nordbotten and M. A. Celia. Similarity solutions for fluid injection into confined aquifers. *J. Fluid Mech.*, 561:307–327, 2006.

[17] Working Group III of the Intergovernmental Panel on Climate Change. *IPCC special report on Carbon Dioxide Capture and Storage*. Cambridge University Press, United Kingdom and New York, NY, USA, 2005.

[18] Ø. Pettersen. *Grunnkurs i RESERVOARMEKANIKK*. Matematisk institutt, Universitetet i Bergen, 1990.

[19] P. Tans. www.esrl.noaa.gov/gmd/cgg/trends, November 2008. Earth System Research Laboratory.